

## ***Supporting Information***

# **Ferrocene-based Porous Organic Polymer Derived N-Doped Porous Carbon/Fe<sub>3</sub>C Nanocrystal Hybrids towards High-efficiency ORR for Zn-air Battery**

Xia Liu,<sup>a†</sup> Xiaoming Liang,<sup>b†</sup> Han Lou,<sup>d</sup> Huiru Wang,<sup>b</sup> Hui Li,<sup>b</sup> Shujuan Zhang,<sup>b</sup> Shourong Zhu,<sup>a</sup>  
Weina Han,<sup>b\*</sup> Baolong Zhou<sup>b,c\*</sup>

<sup>a</sup>*Department of Ophthalmology, Affiliated Hospital of Weifang Medical University, Weifang 261031, Shandong, P. R. China*

<sup>b</sup>*School of Pharmacy, Weifang Medical University, Weifang, 261053, Shandong, P. R. China*

<sup>c</sup>*Shandong Engineering Research Center for Smart Materials and Regenerative Medicine, Weifang Medical University, Weifang, 261053, Shandong, P. R. China.*

<sup>d</sup>*Department of Urology, Affiliated Hospital of Weifang Medical University, Weifang 261031, Shandong, P. R. China*

†These authors make equal contribution to this article.

E-mail: [zhoubalong@wfmc.edu.cn](mailto:zhoubalong@wfmc.edu.cn)

## **Contents**

**Section 1. Materials and Characterization**

**Section 2. Experimental Details**

**Section 3. Electrochemical Measurements and Drug Delivery**

**Section 4. Liquid NMR**

**Section 5. TG.**

**Section 6. SEM and TEM**

**Section 7. XPS**

**Section 8. Electrochemical Performance**

**Section 9. Supporting Tables**

**Section 10. Supporting References**

## Section 1. Materials and Characterization

### Materials

Pyrrole, carbazole,  $\text{Na}_2\text{SO}_4$  and ferrocene were purchased from commercial suppliers and used as received. Hexane was dried over  $\text{CaH}_2$ , and distilled. TMEDA, DMF were dehydrated with active 4 Å molecular sieves. Other chemicals and reagents were also purchased from commercial suppliers without further purification unless otherwise stated.

### Characterization

$^1\text{H}$ , and  $^{13}\text{C}$  NMR spectra of prepared monomers were recorded on an Avance Bruker DPX 400 (400 MHz) in the solvent of  $\text{CDCl}_3$ . Solid-state  $^{13}\text{C}$  CP/MAS NMR were collected on Bruker SB Avance III 500 MHz spectrometer. Fourier Transform Infrared Spectroscopy (FTIR) was performed on KBr pellets in the range from 4000 to 400  $\text{cm}^{-1}$  using Spectrum Spotlingt 400. Thermo-gravimetric analysis (TGA) were recorded using NETZSCH STA 449C analyzer from 25 °C to 900 °C at a heating rate of 10 °C  $\text{min}^{-1}$  under the protection of  $\text{N}_2$ . The morphologies of powder samples were evaluated by field-emission scanning electron Microscopy (FESEM, Ultra 55) and transmission electron microscopy (TEM, Tecnai G2 20 TWIN) via dipping the prepared samples on a Cu-net. The adsorption and desorption measurements for  $\text{N}_2$  were performed on a Belsorp max analyzer (Japan) at low temperature of -273K. Before test, all these samples were degassed overnight under high vacuum at the temperature of 150 °C to remove the solvent or the water absorbed in the porous skeleton. X-ray

Photoelectron Spectroscopy (XPS) was conducted on XPSESCALAB 250Xi analyser. X-ray diffraction (XRD) parameters were obtained using a Rigaku-DMAX 2500 diffractometer at a rate of  $4^{\circ} \text{ min}^{-1}$  from  $5^{\circ}$  to  $80^{\circ}$ .

## Section 2. Experimental Details

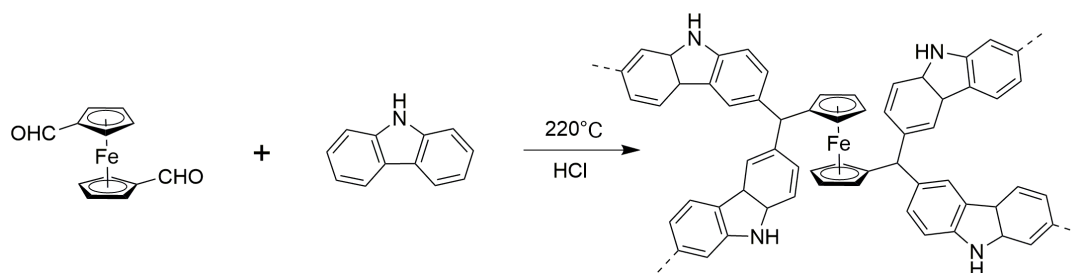
### Preparation of 1,1 -ferrocenecarboxaldehyde



**Scheme S1.** Synthetic routes of 1,1 -ferrocenecarboxaldehyde

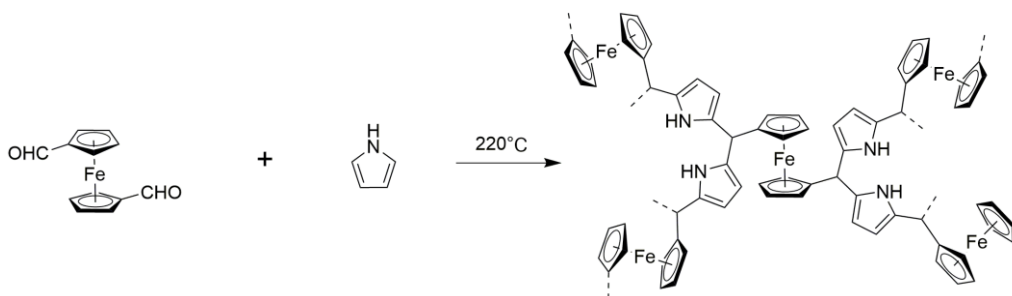
The reaction was carried out in a Schlenk-type apparatus under argon. Ferrocene (5 g, 26 mmol) in 75 ml of dry hexane was treated with 24 mL of 2.5 M  $n$ -butyllithium (60 mmol) in hexane, and subsequent addition of 8.5 ml of tetra-methylethylenediamine (TMEDA) (56 mmol). The reaction mixture was stirred for 20 h, then 6.5 ml of DMF was added dropwise at  $-78^{\circ}\text{C}$ . After 2 h stirring, the mixture was hydrolysed at  $-78^{\circ}\text{C}$ . The organic phase was extracted with  $\text{CH}_2\text{Cl}_2$ , and dried over  $\text{Na}_2\text{SO}_4$ , and the solvent then removed. 1,1 -ferrocenecarboxaldehyde was purified with silica gel column when the flow phase was petroleum and ethyl acetate (5:1). A bright red crystal was obtained (4.15g) with the yield of 63.5%.  $^1\text{H NMR}$  (400 MHz, Chloroform- $d$ )  $\delta$  9.94 (s, 2H), 4.87 (s, 4H), 4.66 (s, 4H).

## Synthesis of Fc-Car



In a round bottom flask, an amount of 0.345 g (2 mmol) of carbazole, 0.242 g of 1,1'-ferrocenecarboxaldehyde (1mmol) and 1 ml of 1 M HCl (2 M) were added to 5 ml of dioxane. The mixture was let to react for one day at 100°C. and transferred to a Teflon lined autoclave which was purged with Ar to remove the air and placed in an oven at 220 °C for 2 days. After cooling at room temperature, a black powder was obtained and was washed three times with THF. The product was dried in a vacuum oven. The yield of the polymerization was 90.6%.

## Synthesis of Fc-Py



In a round bottom flask, an amount of An amount of 0.227ml (4 mmol) of pyrrole and 0.484 g (2mmol) of 1,1'-ferrocenecarboxaldehyde were added to 5ml hexane. The mixture was let to react for 3 hours at 70 °C, then transferred to a Teflon lined autoclave which was purged with Ar to remove the air and placed in an oven at 220 °C for 2 days. After cooling at room temperature, a black powder was obtained and was washed three times with THF. The product was dried in a

vacuum oven. The yield of the polymerization was 82.4%.

### **Synthesis of CF-X.**

FP-X was prepared via direct carbonization of Fc-Por-CMP under the Ar. Briefly, after fine grinding, Fc-Por-CMP was loaded on a porcelain boat and then transferred into a tube furnace. Then, the pyrolysis was conducted under the atmosphere of Ar and heated to the target temperature (X =850, 950 and 1000 °C) for 2 h.

### **Synthesis of FP-DOX.**

DOX and Fc-Py in different mass ratio were suspended in 2 mL water with stirring at room temperature for 8 h. Meantime, The DOX was absorbed into the pores of the POP, and obtaining the final composite, named as FP-DOX.

## **Section 3. Electrochemical Measurements**

All electrochemical tests were performed at room temperature using standard three-chamber cells to record the electrode pairs of platinum grid, and the Ag/AgCl electrode was extremely saturated with KCl. All the potentials were referenced to the reversible hydrogen electrode (RHE) scale according to the Nernst equation, *i. e.*,  $E(\text{RHE}) = E(\text{Ag}/\text{AgCl}) + 0.059 \times \text{pH} + 0.197 \text{ V}$ , at 25°C.<sup>S1</sup>

The working electrode can be either a rotating disk electrode (RDE) composed of a glass carbon disk (diameter 5.0 mm) or a rotating ring disk electrode (RRDE) composed of a glass carbon disk (diameter 3 mm) surrounding an outer platinum ring (inner diameter 5 mm, outer diameter 7 mm). The catalyst ink is loaded on the working electrode surface. The catalyst inks and commercially available Pt/C (20 wt%) inks are made by dispersing 5.0 mg of the fresh-prepared catalyst or

commercially available Pt/C (20 wt%) in an ultrasonic bath to a 500  $\mu\text{L}$  solvent mixture (25  $\mu\text{L}$  Naffion solution (5 wt%), 75  $\mu\text{L}$   $\text{H}_2\text{O}$ , and 400  $\mu\text{L}$  ethanol) to a uniform suspension. Then suck the catalyst ink (8  $\mu\text{L}$ ) through a straw onto the glass carbon surface of RDE or RRDE and let it dry in the air at room temperature.

The catalytic activity of the catalyst was measured by cyclic voltammetry (CV) and rotary disk electrode (RDE) at CHI-760 electrochemical station. All tests were carried out under alkaline (0.1 M KOH), neutral (0.1 PBS), or acidic conditions (0.1M  $\text{HClO}_4$ ). CV was measured at 50  $\text{mV s}^{-1}$  in various electrolytes saturated with  $\text{O}_2$  or Ar. The RDE/RRDE tests were examined with a scanning rate of 5  $\text{mV s}^{-1}$  at different speeds ranging from 400 to 2500 rpm. The K-L equation was applied to investigate the ORR kinetic parameters. The K-L equation can be described as follows:

$$\frac{1}{J} = \frac{1}{J_L} + \frac{1}{J_K} = \frac{1}{B \omega^{1/2}} + \frac{1}{J_K} \quad (1)$$

Where  $J$  is the current density,  $J_L$  is the current that was measured;  $J_K$  represents the kinetic-limiting current and  $\omega$  is the rotation speeds of electrode.

$$B = 0.62nFC_0(D_0)^{2/3}V^{-1/6} \quad (2)$$

In equation 2,  $n$  is the total number of transferred electrons during the oxygen reduction process;  $F$  is Faradaic constant ( $F = 96485 \text{ C mol}^{-1}$ ),  $C_0$  is the  $\text{O}_2$  concentration (solubility) in 0.1 M KOH electrolyte ( $1.2 \times 10^{-6} \text{ mol cm}^{-3}$ );  $D_0$  is the  $\text{O}_2$  diffusion coefficient ( $1.90 \times 10^{-5} \text{ cm}^2 \text{ s}^{-1}$ ), and  $V$  is the kinematic viscosity of the  $\text{O}_2$  saturated 0.1 M KOH solution ( $0.01 \text{ cm}^2 \text{ s}^{-1}$ ). For the RRDE measurements, the disk electrode was also scanned with a rate of 5  $\text{mV s}^{-1}$  at a

constant ring potential of 1.5 V vs. RHE. The peroxide percentage ( $H_2O_2$  yields) and the transferred number of electron ( $n$ ) were calculated according to the following equations (3) - (4):

$$H_2O_2\% = 200 \frac{I_r/N}{I_d + I_r/N} \quad (3)$$

$$N = 4 \frac{I_d}{I_d + I_r/N} \quad (4)$$

In equation 3 and 4,  $I_d$  is the disk current, and  $I_r$  refers to the ring current and N represents the current collection efficiency of the Pt ring ( $N=0.4581$ ).

#### Section 4. Liquid NMR

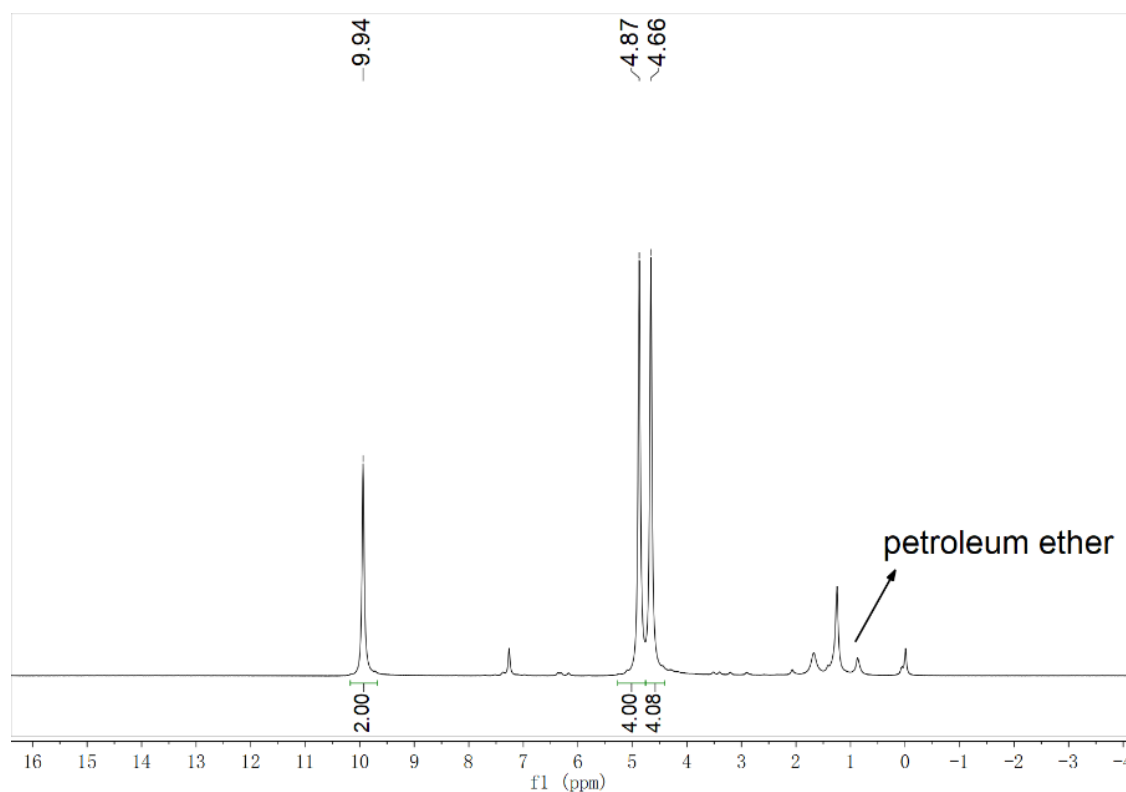


**Figure S1.**  $^1H$  NMR of 1,1'-Ferrocenedicarboxaldehyde.

## Section 5. TG.

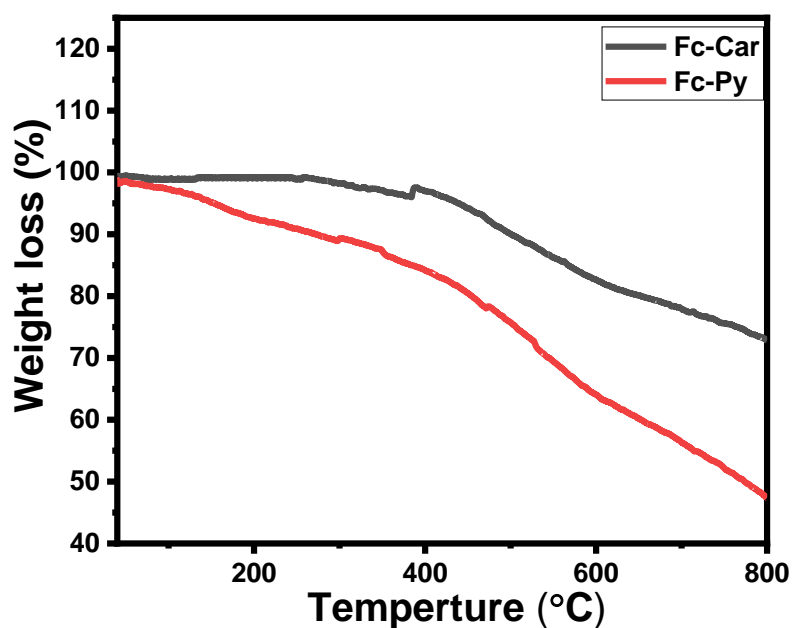


**Figure S2.** TG of prepared polymers.

The evolution process from the amorphous POPs to the Fe/Fe<sub>3</sub>C@Carbon shell could be explained from the thermal gravity analysis. The main weight loss occurs over two different temperature ranges. The mild weight loss occurred in the temperature below 400 °C can be attributed to the evaporation of absorbed water in the porous skeletons; the next loss in the high temperature is attributed to the decomposition of N-rich rigid porous polymers with uniformly doped Fe species that released the nitrogen containing gas for carbide reaction Nitrogen doping. Meanwhile, the Fe served as the catalysts which could accelerate the generation of Fe/Fe<sub>3</sub>C particles and growth of graphite layer, simultaneously.

## Section 6. SEM and TEM

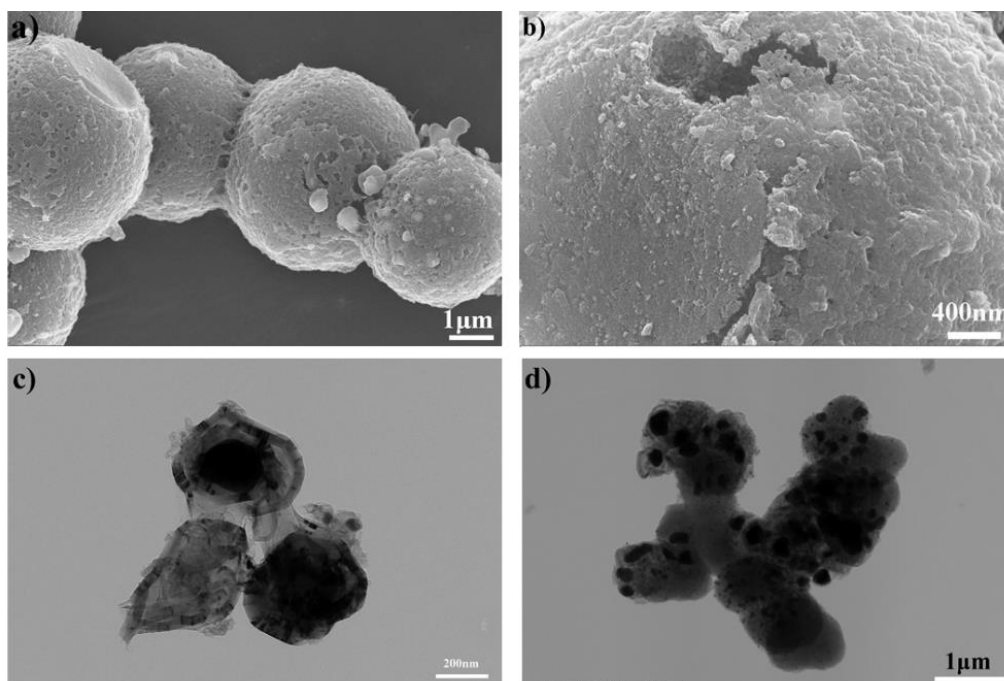


**Figure S3.** SEM and TEM of FC-950. a) SEM of FC-950 at a scale bar of 1  $\mu\text{m}$ ; b) SEM of FC-950 at a scale bar of 400 nm; c) TEM of FC-950 at a scale bar of 200 nm; d) TEM of FC-950 at a scale bar of 1  $\mu\text{m}$ .

## Section 7. X-ray Photoelectron Spectra (XPS)

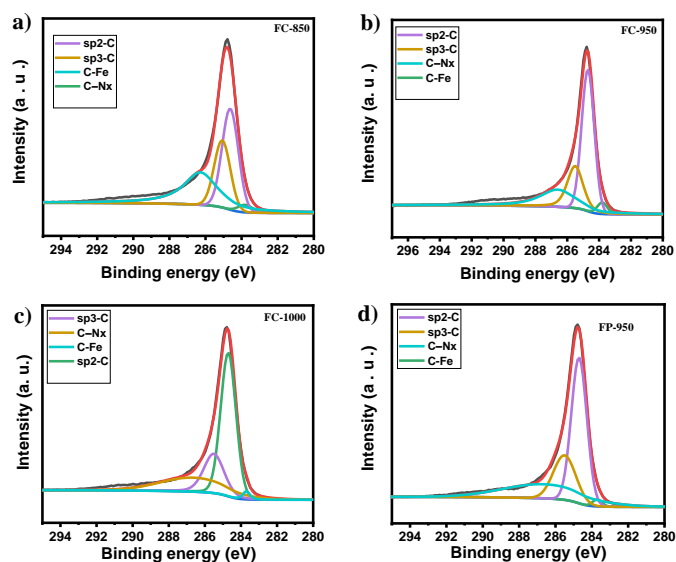


**Figure S4.** High resolution XPS C 1s of as-synthesized materials. a) FC-850; b) FC-950; c) FC-1000; d) FP-950.

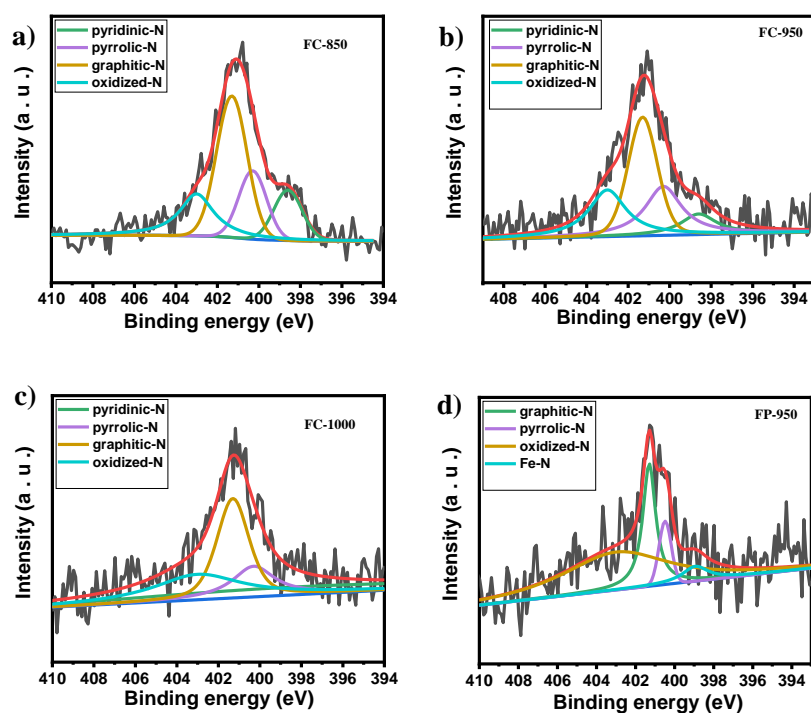


**Figure S5.** High resolution XPS N 1s of as-synthesized materials. a) FC-850; b) FC-950; c) FC-1000; d) FP-950.

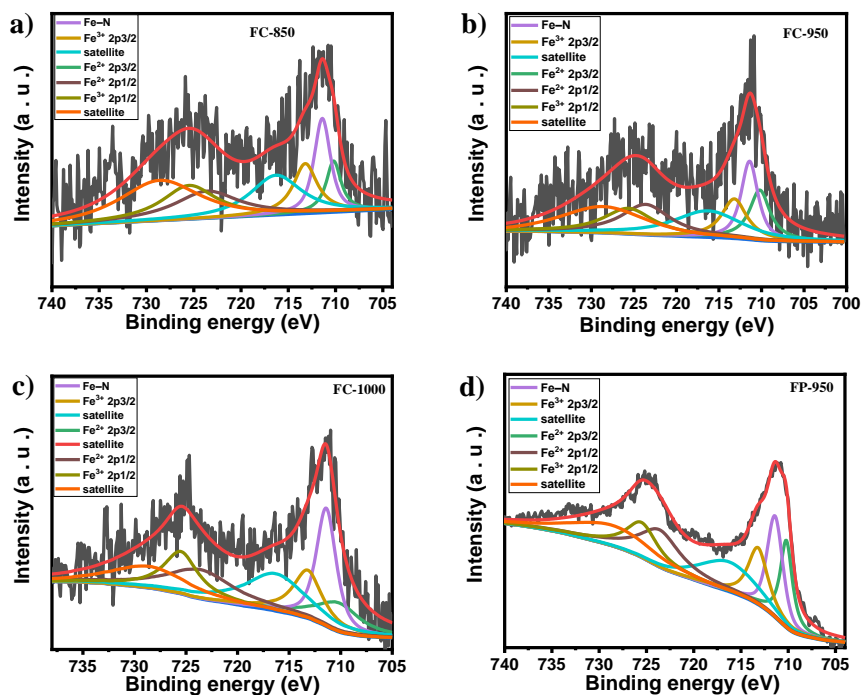


**Figure S6.** High resolution XPS Fe 2p of as-synthesized materials. a) FC-850; b) FC-950; c) FC-1000; d) FP-950.

## Section 8. Electrochemical Performance

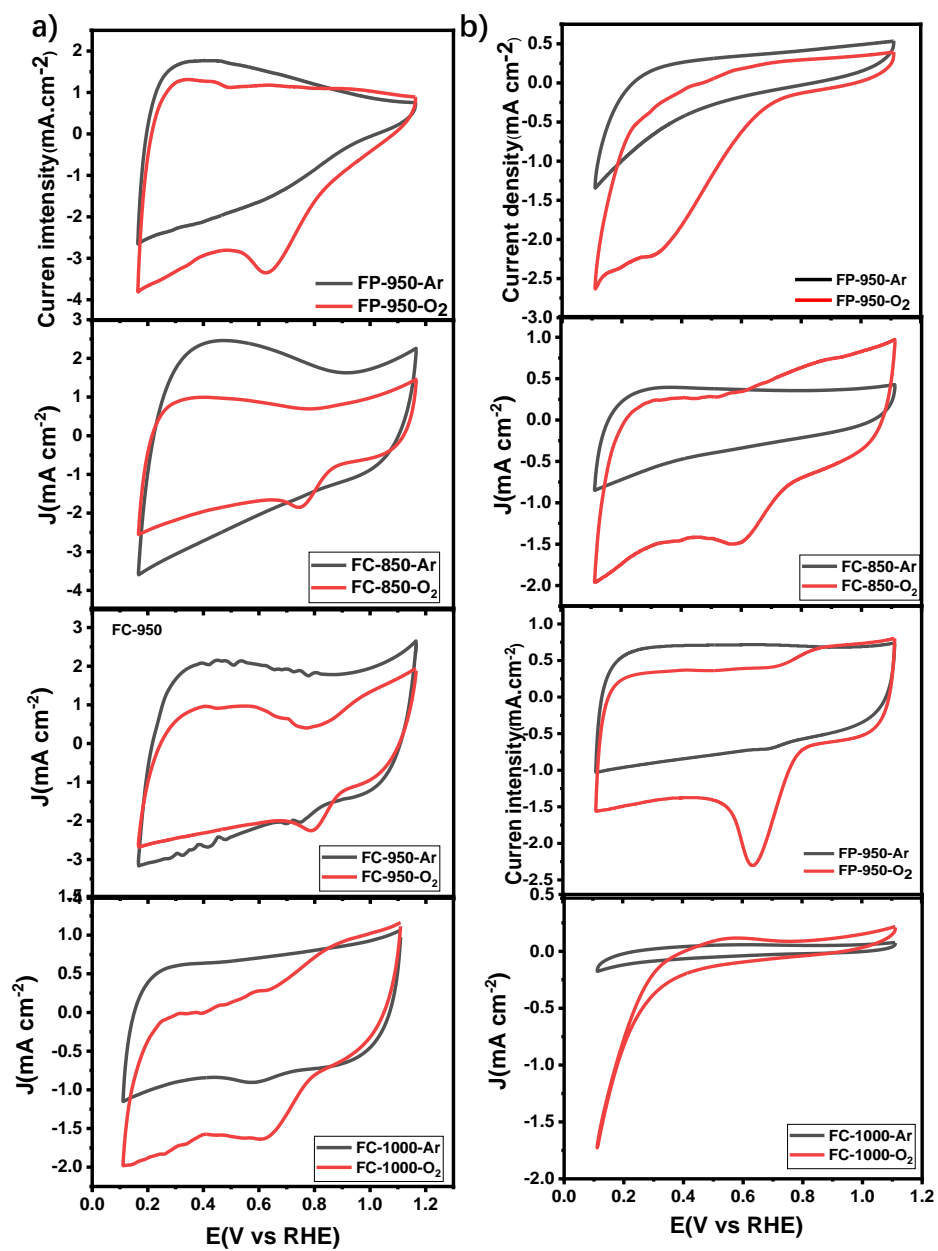


**Figure S7.** CV curves of prepared samples. a) CV curves prepared catalysts in alkaline conditions; b) CV curves of prepared catalysts.

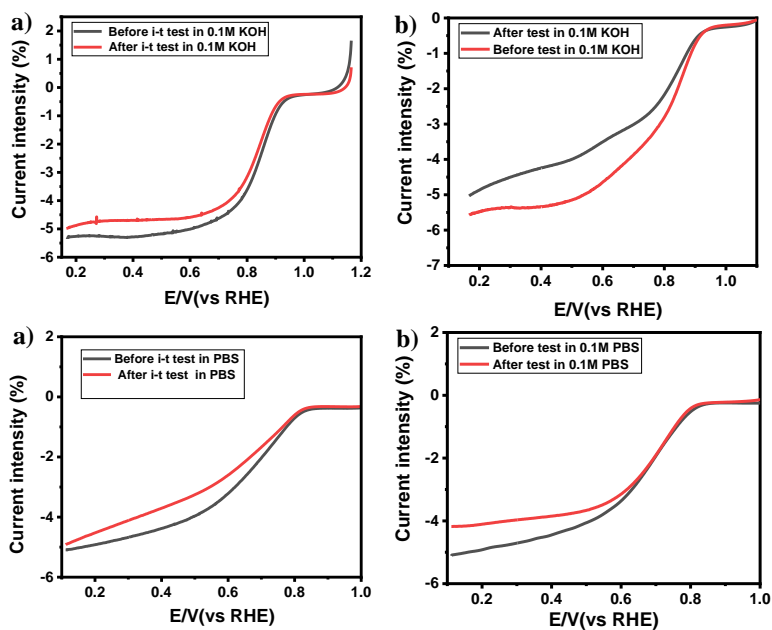


**Figure S8.** LSV curves measured before and after the stability tests or methanol tolerance tests. a) LSV curves of FC-950 measured before and after the stability for 20000 s in 0.1 M KOH saturated with O<sub>2</sub>; b) LSV of FC-950 measured before and after the methanol tolerance tests in 0.1 M KOH; c) LSV curves of FC-950 measured before and after the stability for 20000 s in 0.1 M PBS saturated with O<sub>2</sub>; d) LSV of FC-950 measured before and after the methanol tolerance tests in 0.1 M PBS.

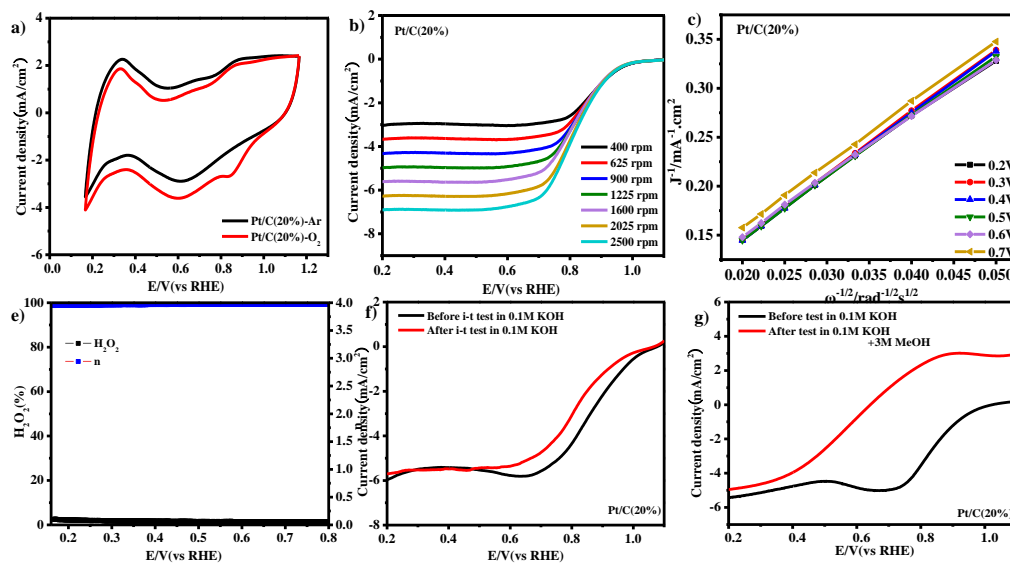


**Figure S9.** a) CV curves of commercial Pt/C (20%) in 0.1 M KOH saturated with O<sub>2</sub> or Ar at a sweep rate of 50 mV s<sup>-1</sup>; b) LSV of commercial Pt/C (20%) at various rotation speeds; c) K-L plots curves of commercial Pt/C (20%); d) Percentage of hydrogen peroxide yield and the electron transfer number (n) of Pt/C at different potentials; e) Polarization curves of Pt/C (20%) measured by RDE in O<sub>2</sub>-saturated 0.1 M KOH before (red line) and after (black line) the i-t (20000 s) experiments; f) LSV curve of Pt/C measured before and after the injection of 3 M methanol.

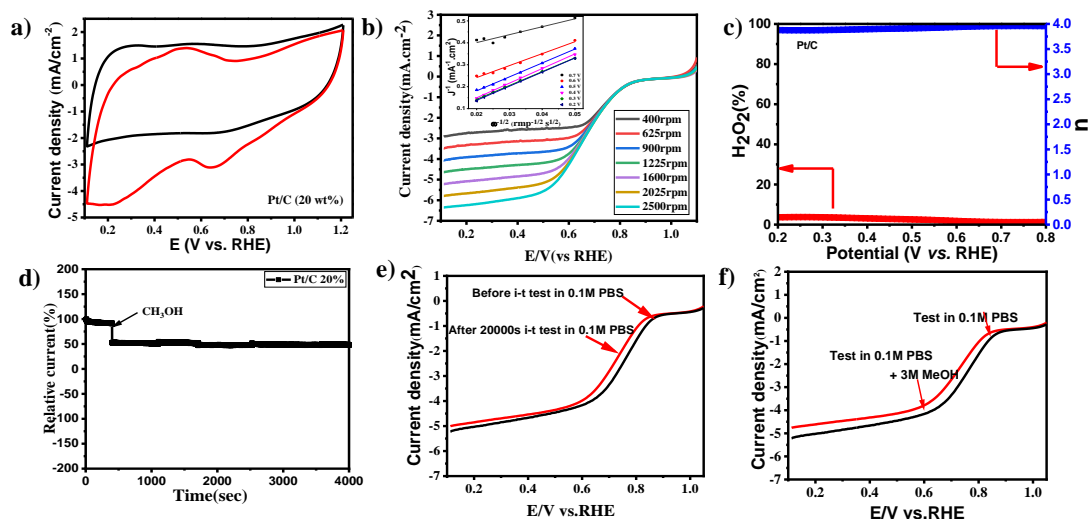


**Figure S10.** Electrochemical performance of Pt/C measured in neutral conditions.

a) CV curves of commercial Pt/C (20%) 0.1 M PBS saturated with O<sub>2</sub> or argon at a sweep rate of 50 mV s<sup>-1</sup>. b) LSV of commercial Pt/C (20%) at different rotation speeds, the insert part is the K-L plots fitting curves of Pt/C (20%) at different potentials; c) Percentage of hydrogen peroxide yield and the electron transfer number (n) of Pt/C (20%) at different potentials; d) Chronoamperometric response of commercial Pt/C at around E<sub>1/2</sub> in O<sub>2</sub>-saturated PBS at 1600 rpm and the methanol was added at 400s; e) Polarization curves of Pt/C (20%) measured by RDE in O<sub>2</sub>-saturated 0.1 M PBS before (red line) and after (black line) the i-t (20000 s) experiments; f) LSV curve of Pt/C (20%) measured before and after the injection of 3 M methanol.

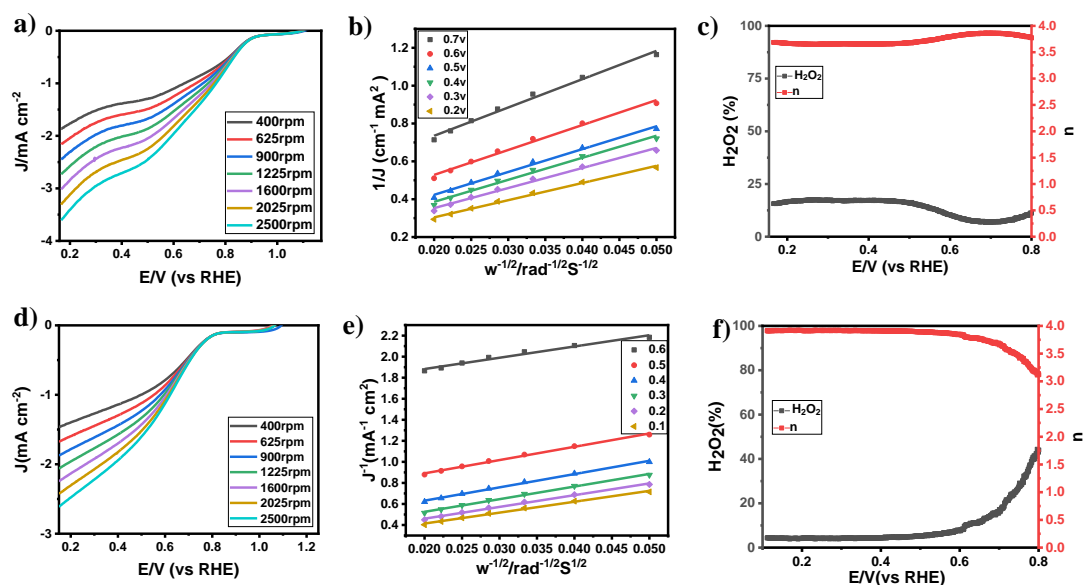


**Figure S11.** Electrochemical performance of FC-850 in alkaline and neutral conditions. a) LSV at different rotation speeds in water solution of 0.1 M KOH; b) K-L plots in water solution of 0.1 M KOH; c) Percentage of hydrogen peroxide yield and the electron transfer number (n) in water solution of 0.1 M KOH at different potentials; d) LSV in water solution of 0.1 M PBS at different rotation speeds; e) K-L plots in water solution of 0.1 M PBS; f) Percentage of hydrogen peroxide yield and the electron transfer number (n) in water solution of 0.1 M PBS at different potentials.

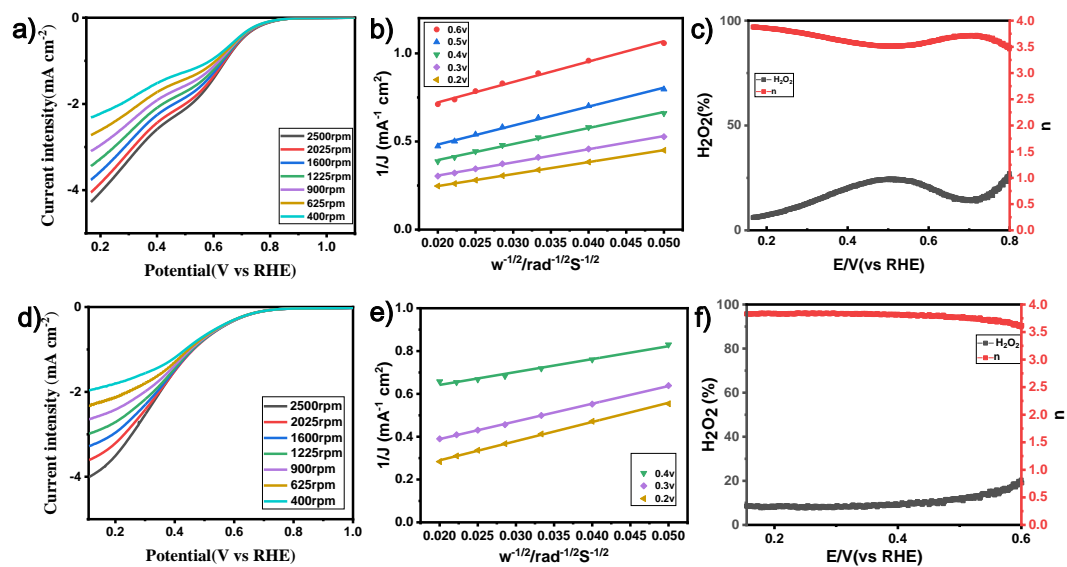


**Figure S12.** Electrochemical performance of FC-1000. a) LSV at different rotation speeds in water solution of 0.1 M KOH; b) K-L plots in water solution of 0.1 M KOH; c) Percentage of hydrogen peroxide yield and the electron transfer number ( $n$ ) in water solution of 0.1 M KOH at different potentials; d) LSV in water solution of 0.1 M PBS at different rotation speeds; e) K-L plots in water solution of 0.1 M PBS; f) Percentage of hydrogen peroxide yield and the electron transfer number ( $n$ ) in water solution of 0.1 M PBS at different potentials.

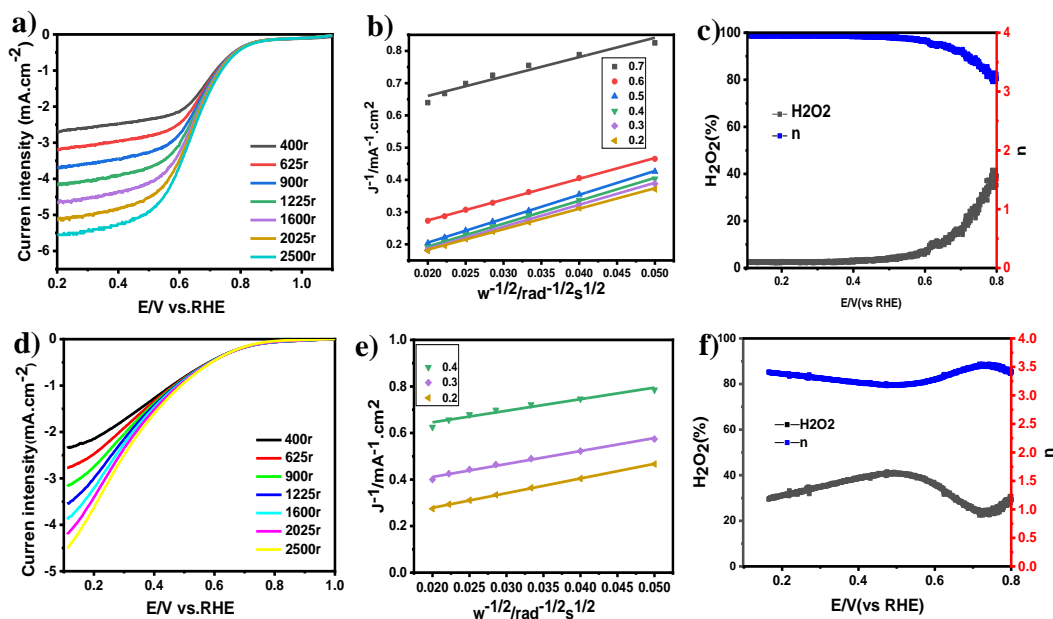


**Figure S13.** Electrochemical performance of FP-950. a) LSV at different rotation speeds in water solution of 0.1 M KOH; b) K-L plots in water solution of 0.1 M KOH; c) Percentage of hydrogen peroxide yield and the electron transfer number (n) in water solution of 0.1 M KOH at different potentials; d) LSV in water solution of 0.1 M PBS at different rotation speeds; e) K-L plots in water solution of 0.1 M PBS; f) Percentage of hydrogen peroxide yield and the electron transfer number (n) in water solution of 0.1 M PBS at different potentials;

## Section 13. Supporting Tables

**Table S1. Porosity Parameters of prepared polymers and corresponding catalysts.**

Sample	$S_{\text{BET}}$ (m <sup>2</sup> /g)	$V_{\text{Total}}$ (cm <sup>3</sup> /g)	Pore size (DFT) nm
Fc-Py	182	0.13	0.66/1.17/1.72/2.07
Fc-Car	589	0.30	0.6965/0.879/1.63/2.11
FC-850	378	0.19	0.65/0.887/1.69/2.04
FC-950	409	0.23	0.58/0.694/0.891/1.587/2.57
FC-1000	672	0.26	0.694/1.07/1.60

**Table S2. The surface element contents of different species including carbon, oxygen, nitrogen and iron in as-synthesized catalysts, calculated from the XPS spectra**

Sample	C (at%)	O (at%)	Fe (at%)	N (at%)
<b>FC-850</b>	92.78	4.66	0.36	2.20
<b>FC-950</b>	93.71	4.07	0.37	1.85
<b>FC-1000</b>	93.18	4.82	0.55	1.45
<b>FP-950</b>	90.92	5.33	2.27	1.28

**Table S3. The surface N contents of different species calculated from the XPS spectra**

Sample	Pyridine N in total N (%)	Pyrrolic-N in total N (%)	Graphitic- N in total N (%)	Oxidized N in total N (%)
<b>FP-950</b>	16.2	9.97	26.26	47.55
<b>FC-850</b>	10.89	19.75	45.32	23.99
<b>FC-950</b>	11.65	24.98	45.14	18.20
<b>FC-1000</b>	32.76	14.19	29.15	23.88

**Table S4. Main parameters of the prepared catalysts combined with the commercial Pt/C catalysts in alkaline conditions**

Sample	On-set Potential (E <sub>onset</sub> , V)	Half-wave potential (E <sub>1/2</sub> , V)	Limited Current density (mA cm <sup>-2</sup> )	Electron transfer number (n, at 0.5 V)
<b>FC-950</b>	1.01	0.841	5.29	3.92
<b>FP-950</b>	0.954	0.604	2.73	3.91
<b>FC-850</b>	0.957	0.655	2.86	3.79
<b>FP-1000</b>	0.732	0.609	3.56	3.73
<b>Pt/C(20%)</b>	0.997	0.825	5.620	3.97

**Table S5. Main parameters of the prepared catalysts combined with the commercial Pt/C catalysts in neutral conditions**

Sample	On-set Potential (E <sub>onset</sub> , V)	Half-wave potential (E <sub>1/2</sub> , V)	Current density (mA cm <sup>-2</sup> ; at 0.5V)	Electron transfer number (n, at 0.5 V)
<b>FC-950</b>	0.842	0.61	5.13	3.94
<b>FP-950</b>	0.775	0.57	1.73	3.90
<b>FC-850</b>	0.80	0.59	2.27	3.84
<b>FC-1000</b>	0.711	0.41	3.31	3.76
<b>Pt/C(20%)</b>	0.844	0.67	5.44	3.95

**Table S6. Summarized properties of our and some previously reported Zn-air batteries with Zn(Ac)<sub>2</sub> and KOH as the electrolytes.**

Catalysts	Open-circuit (V)	Power density (mW cm <sup>-2</sup> )	Discharge potential (V)	Ref.
<b>FC-950</b>	1.452	176.8	1.18	This work
<b>C-MOF-C2-900</b>	1.46	105	1.28	S1
<b>h-FeNC</b>	1.6	215	---	S2
<b>FeS/Fe<sub>3</sub>C@N-S-C-800</b>	1.44	61	0.85	S3
<b>Co<sub>2</sub>P@am-FePO<sub>4</sub></b>	1.395	152	1.09	S4
<b>meso/micro-FeCo-Nx-CN-30</b>	1.40	150	1.26	S5
<b>TF-C-900</b>	1.3	243	1.26	S6
<b>CoFe/NGCT</b>	1.43	203	1.24	S7
<b>Fe/Fe<sub>3</sub>C@N-C</b>	1.43	102	1.22	S7
<b>Fe/Fe<sub>3</sub>C@NCNTs</b>	1.47	198	1.10	S8
<b>Fe/Fe<sub>3</sub>C@Fe-Nx-C</b>	1.44	147	1.23	S9

## Section 10. Supporting References

- S1. M. Zhang, Q. Dai, H. Zheng, M. Chen, and Liming Dai, *Adv. Mater.* **2018**, 1705431.
- S2. R. Dun, M. Hao, Y. Su and W. Li, *J. Mater. Chem. A*, **2019**, 7, 12518.
- S3. F. Kong, X. Fan, A .Kong, Z. Zhou, X. Zhang, and Y. Shan, *Adv. Funct. Mater.* **2018**, 1803973.
- S4. D. Cheng, Z. Wang, C. Chen, and K. Zhou, *Chem. Mater.* **2019**, 31, 8026.
- S5. S. Li, C. Chen, X. Zhao, J. Schmidt, and A. Thomas, *Angew. Chem. Inter. Ed.*, **2018**, 57, 1856.
- S6. B. Zhou, L. Liu, Z. Yang, X. Li, Z. Wen, and L. Chen, *ChemElectroChem* **2019**, 6, 485.
- S7. X. Liu, L. Wang, P. Yu, C. Tian, F. Sun, J. Ma, W. Li, and H. Fu, *Angew.Chem. Int. Ed.* **2018**, 57, 16166.
- S8. Y. Xu, B. Zhang, J. Ran, P. Liu, and D. Gao, *Nanotechnology*, **2020**, 31, 265402.
- S9. L. Zong, X. Chen, S. Liu, K. Fan, S. Dou, J. Xu, X. Zhao, W. Zhan, Y. Zhang, W. Wu, F Lu, L. Cui,
- X. Jia, Q. Zhang, Y. Yang, J. Zhao, X. Li, Y. Deng, Y. Chen, L. Wang, *J. Energy Chem.* **2021**, 56, 72.